

# Live Cell Refractometry Using Hilbert Phase Microscopy and Confocal Reflectance Microscopy<sup>†</sup>

Niyom Lue,<sup>‡</sup> Wonshik Choi,<sup>\*,§</sup> Gabriel Popescu,<sup>||</sup> Zahid Yaqoob,<sup>‡</sup> Kamran Badizadegan,<sup>‡,⊥</sup> Ramachandra R. Dasari,<sup>‡</sup> and Michael S. Feld<sup>‡</sup>

G. R. Harrison Spectroscopy Laboratory, Massachusetts Institute of Technology, Cambridge, Massachusetts 02139, Department of Physics, Korea University, Seoul 136-701, Korea, Department of Electrical and Computer Engineering, University of Illinois at Urbana–Champaign, Urbana, Illinois 61801, and Department of Pathology, Harvard Medical School and Massachusetts General Hospital, Boston, Massachusetts 02114

Received: May 20, 2009; Revised Manuscript Received: September 15, 2009

Quantitative chemical analysis has served as a useful tool for understanding cellular metabolisms in biology. Among many physical properties used in chemical analysis, refractive index in particular has provided molecular concentration that is an important indicator for biological activities. In this report, we present a method of extracting full-field refractive index maps of live cells in their native states. We first record full-field optical thickness maps of living cells by Hilbert phase microscopy and then acquire physical thickness maps of the same cells using a custom-built confocal reflectance microscope. Full-field and axially averaged refractive index maps are acquired from the ratio of optical thickness to physical thickness. The accuracy of the axially averaged index measurement is 0.002. This approach can provide novel biological assays of label-free living cells in situ.

## 1. Introduction

Absorption measurements are widely used in spectrophotometry for chemical analysis of molecules.<sup>1–3</sup> The Beer–Lambert law enables one to extract the absorption coefficient, a quantity proportional to the molecular number density and absorption cross section.<sup>4</sup> With known molecular specific absorption cross section, the molecular concentration can be determined. A similar approach can be developed using the refractive index instead of absorption coefficient. This complementarity between the refractive and absorption properties of materials stems from the fact that they represent the imaginary and real part of the material dielectric response function and, thus, are related via a Kramers–Kronig relationship. As is widely known, the refractive index is also linearly proportional to the concentration of molecules.<sup>5</sup> Molecular concentrations thus can be determined from optical phase delay measurements with known physical path length. The absorption approach requires tuning the wavelength of light to the resonance to maximize the signal-to-noise ratio. In contrast, highly accurate phase detection provides enough detection sensitivity of refractive index even when the absorption is insignificant. Thus the refractive index approach is preferable where photodamage is of concern.

The spectrophotometry typically uses a cuvette to predetermine the thickness of a specimen through which light travels. In studying samples of arbitrary shapes with significant dynamics such as live biological cells, the thickness can vary continuously over time. This makes it difficult to detect absorption coefficient or refractive index in situ. Here we introduce a technique that can be used to determine the refractive index of an arbitrarily shaped specimen by means of optical

microscopy. Our method will lead to the study the dynamics of protein concentrations in living biological cells.

The refractive index has been an important source of contrast in visualizing living cells because different cell organelles and compartments possess different refractive indices. Phase-sensitive microscopy techniques such as phase contrast microscopy and differential interference microscopy<sup>6,7</sup> visualize minute spatial differences in indices and thus provide high-contrast cellular images. However, these traditional techniques provide only *qualitative* information. Recently, advanced phase microscopy techniques have been used to *quantify* the cellular refractive index.<sup>9–14</sup> From this information, chemical content such as average hemoglobin concentration and average cell mass can be readily extracted.<sup>8,9</sup> In previous studies it was demonstrated that refractive index can be used to determine biomolecular contents without such artifacts as photobleaching and interference on the normal physiological activities of living specimen typically present in chemical staining.

Several methods have been used to measure the refractive index of living cells. One of the most advanced methods is tomographic phase microscopy, which can determine 3D maps of refractive index.<sup>10</sup> But the technique may not be readily available to general biology laboratories. Moreover, there can be many applications requiring only average refractive index, and not the detailed 3D maps.

Hilbert phase microscopy (HPM)<sup>11</sup> is a quantitative phase imaging method that can be used to acquire the axially averaged refractive index of cells when the thickness is known.<sup>12</sup> Since quantitative phase measurements provide only optical thickness, a phase shift induced by a specimen proportional to both the average index and the physical thickness, it is required to independently measure the physical thickness of the specimen to extract an average refractive index. To obtain the knowledge of cell thickness, we previously constrained the cells into a known dimensional microstructure.<sup>12</sup> Another approach was to dissociate cells from a substrate to make the shape of cells

<sup>†</sup> Part of the “Robert W. Field Festschrift”.

\* Corresponding author. E-mail: wonshik@mit.edu.

<sup>‡</sup> Massachusetts Institute of Technology.

<sup>§</sup> Korea University.

<sup>||</sup> University of Illinois at Urbana–Champaign.

<sup>⊥</sup> Harvard Medical School and Massachusetts General Hospital.

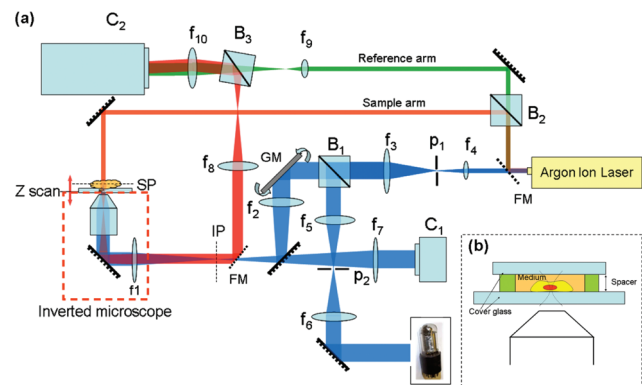


**Figure 1.** (a) Experimental setup. IP and SP are image and sample plane. GM indicates dual-axes galvanometer mirrors. FMs: flip mirrors. B1, B2, and B3 are beam splitters.  $f_1$  is a tube lens.  $f_2$ – $f_6$  are convex lenses with focal length of 200 mm.  $f_7$ – $f_{10}$  are convex lenses with focal length of 250, 150, 50, and 150 mm. C1 and C2 are video monitoring camera and CCD camera. (b) Sample chamber. Cells were positioned in a chamber made up of a spacer and cover glasses.

approximately spherical.<sup>12</sup> Further, it has been proposed to image the optical thickness of a given biological cell at two different media with different refractive indices, either by a perfusion of different media or by use of dye-induced dispersion.<sup>13,14</sup> Confocal fluorescence microscopy was used to directly measure the physical thickness of the cells.<sup>15</sup> However, all the techniques require either physical perturbation or chemical staining such as fluorescence dyes, which may introduce changes in actual refractive index.

We note that confocal reflectance microscopy can provide the physical contour of the cell without staining.<sup>16–18</sup> The technique preserves the refractive indices of native cells and, at the same time, offers high resolution cell thickness maps due to its sectioning capability. Thus, this technique can be a good complement to quantitative phase microscopy. In this report, we combine the confocal reflectance microscopy with Hilbert phase microscopy to obtain the refractive index of cells without any assumptions, constraint and exogenous agents. We demonstrate full-field imaging of axially averaged refractive index map in live cells.

## 2. Experimental Section

**Hilbert Phase Microscopy.** The setup (Figure 1a) used an inverted microscope (Axiovert 100 Zeiss, Germany) as a platform. The illumination source (Argon Ion Laser, 35 IMA 040-120, Melles Griot) with wavelength of 488 nm was split into reference and sample arms by a beam splitter (B2) to construct a Mach–Zehnder interferometer. The sample beam traveled through a sample and entered the inverted microscope. The image of the sample was relayed to the image plane (IP) via objective (Zeiss 100x, 1.3 NA, oil immersion) and tube lens. Using  $f_8$  and  $f_{10}$  lenses the image was relayed to the camera plane, which gave overall magnification of 160. The reference beam, unlike the sample beam, traveled outside of the microscope and passed through  $f_9$  and  $f_{10}$  lenses before it was brought to interfere with the sample arm by a beam splitter cube (B3) at the camera plane. The interference fringes, which contain information of the sample-induced phase shifts, were digitally captured by a CCD camera (C7770, Hamamatsu Photonics, Japan), which has  $640 \times 480$  square pixels,  $9.9 \times 9.9 \mu\text{m}^2$  pixel size. To maximize the number of fringes, the beam splitter cube (B3) was positioned in such a way that the interference fringes were oriented  $45^\circ$  with respect to the horizontal axis of the CCD

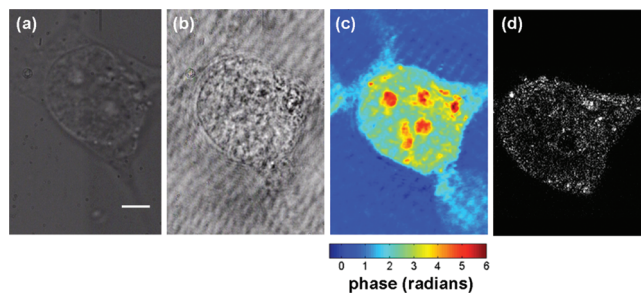


**Figure 2.** (a) Bright field image of a HeLa cell with oblique illumination. (b) Intensity image acquired by HPM. (c) Phase image taken by HPM image. Color bar indicates phase in radians. (d) Confocal reflectance image at a specific focal plane. The scale bar indicates  $5 \mu\text{m}$ .

camera. The intensity distribution of the interference image recorded by the HPM technique is given by

$$I(x,y) = I_{\text{obj}} + I_{\text{ref}} + 2\sqrt{I_{\text{obj}}I_{\text{ref}}}\cos(\Delta\Phi_{\text{obj}} + \Phi_{\text{bg}} + q_x x + q_y y) \quad (1)$$

where  $q_x$  and  $q_y$  are the spatial frequencies of the fringes in the  $x$  and  $y$  axes, respectively.  $I_{\text{obj}}$  and  $I_{\text{ref}}$  are the intensities of the sample and reference beams, and  $\Delta\Phi_{\text{obj}}$  and  $\Phi_{\text{bg}}$  are the sample induced phase delay and the phase difference between the reference and sample beams. Using high-pass spatial filtering and the Hilbert transformation, we obtained  $\Delta\Phi_{\text{obj}} + \Phi_{\text{bg}}$ . By taking an interference image with no sample in the field of view, we measured the reference phase  $\Phi_{\text{bg}}$ . By subtracting this background phase from the previously measured phase image with sample, we obtained the sample induced phase delay. 2D phase unwrapping algorithm based on the Goldstein method by Ghiglia and Pritt<sup>20</sup> was carried out to eliminate phase ambiguity. Note that this HPM processing details are also described elsewhere.<sup>19</sup>

Figure 2b shows an intensity image of a HeLa cell,  $I_{\text{obj}}$ , with coherent illumination, which was obtained by blocking the reference arm during an interference measurement, and Figure 2c shows the quantitative phase image of the HeLa cell. The sensitivity of phase detection was around 10 mrad. For monitoring purpose, bright field images (Figure 2a) were acquired using a white LED (PJ-1505, CCS Inc. (not shown in Figure 1a) as an illumination source. The image was recorded by a CCD camera (CC35ED, Sony Japan). Note that an oblique illumination technique known as diffracted-light contrast enhancement<sup>21</sup> was used to enhance the contrast of the image.

**Confocal Reflectance Microscopy.** The same argon ion laser was used as an illumination source for confocal reflectance microscopy (Figure 1a). Two flip mirrors (FMs) were switched off to guide the illumination beam through the confocal microscopy setup. The high numerical aperture objective lens (Zeiss 100x, 1.3 NA) can provide diffraction-limited lateral resolution of  $0.61\lambda/2^{1/2}NA = 162 \text{ nm}$ .<sup>22,23</sup> An excitation-pinhole (P1),  $50 \mu\text{m}$  in diameter, was placed at the focal plane of a lens ( $f_4$ ). After the pinhole, the transmitted beam was collimated by a lens,  $f_3$ . The illumination spot at the sample was scanned by dual-axis galvanometer mirrors (Model 6732, Cambridge Technology). The beam reflected from the galvanometer mirror was focused by a lens,  $f_2$ , to an image plane (IP), which later was relayed to the sample plane (SP) through tube and objective lenses. The point beam thereby was focused on a sample and was scattered due to the local heterogeneity of refractive index.

The scattered beam was collected by the same objective lens and was traced back through the incoming path and descanned by galvanometer mirrors. The scattered field from the sample was reflected at a beam splitter (B1) and was focused by a lens,  $f_5$ , to a detection-pinhole (P2,  $30\ \mu\text{m}$  in diameter) which rejects scattered lights originated outside of the focal spot. The size of the detection pinhole was selected to be slightly larger than the diffraction limit to acquire adequate signals for the photomultiplier tube (R6357, Hamamatsu Japan). As a result, the size of the detection pinhole posed an experimental limit in the lateral resolution and the measured resolution was about  $300\ \text{nm}$ , which was validated from the edge response function fit of a USAF target image. We also validated the axial resolution of about  $1\ \mu\text{m}$ . A lens ( $f_6$ ) expanded the beam to fill up an aperture of the photomultiplier tube (PMT, R6357, Hamamatsu) to maximize the detection efficiency. The photoelectric signal from PMT was amplified by a preamplifier (C7319, Hamamatsu). Axial scanning was accomplished by a motorized translation stage (PI M126-DG1, Physik Instrumente, Germany). A data acquisition board (PCI-6251) and Labview software (National Instruments) were used for controlling galvanometer mirrors, translation stage, and recording photoelectric signals from the PMT. The focused beam was scanned at the rate of  $100\ \text{kHz}$ . As a result, it took  $1.6\ \text{s}$  to record one lateral image composed of  $400 \times 400$  pixels ( $\sim 30 \times 30\ \mu\text{m}$ ). To acquire the entire cell profile, 3D scanning was performed in an axial step of  $85\ \text{nm}$ . This typical 3D measurement was accomplished in less than  $5\ \text{min}$ . The confocal reflectance signal detected by the PMT was displayed as a function of the position of the scanning beam. Figure 2d shows the lateral confocal reflectance image of the same cell shown in Figure 2a–c at a specific focus. Due to the heterogeneity of the refractive index, the distribution is somewhat granular. Nevertheless, the cell boundary as well as some internal structures is clearly visible.

**Sample Preparation.** HeLa cell, an immortal cell line derived from cervical cancer cells, was used in this study. Cells were cultivated from cryo-preservation and replanted for several generations to ensure the cells' viability. Cells were cultured in Dulbecco's Modified Eagle Medium (DMEM) with 5% Fetal Bovine Serum (FBS) and penicillin-streptomycin (Gibco). In this experiment, cells were replanted in an imaging chamber made up of a secure seal spacer (Electron Microscopy Sciences) and cover glasses of thickness No. 1 (Figure 1b). Cells were incubated for  $48\ \text{h}$  to allow them to attach to the glass substrate before the measurements. This helped to minimize the cell's movement during the data collection process.

### 3. Data Analysis and Results

From the confocal images acquired from various focal planes, we constructed 3D images of HeLa cells by applying built-in MATLAB (Mathworks, Inc.) functions such as edge detection, image dilation and erosion. Figure 3a shows three perpendicular plane images of a recorded 3D confocal image, where  $x$  and  $y$  axes are in the lateral plane and  $z$  corresponds to the axial direction. The index mismatch between the cell medium and immersion oil for the objective lens induces discrepancies between the scan distance of a sample and the displacement of a focus beam.<sup>19</sup> From the refractive index of immersion oil,  $1.51$ , and cell,  $1.37$ , the effective movement of the focused beam was calculated to be  $0.6$  times the sample's scan distance. This factor was included in the 3D reconstruction of confocal image. Figure 3b displays an estimated thickness map of a HeLa cell from the reconstructed 3D confocal data with the color bar in

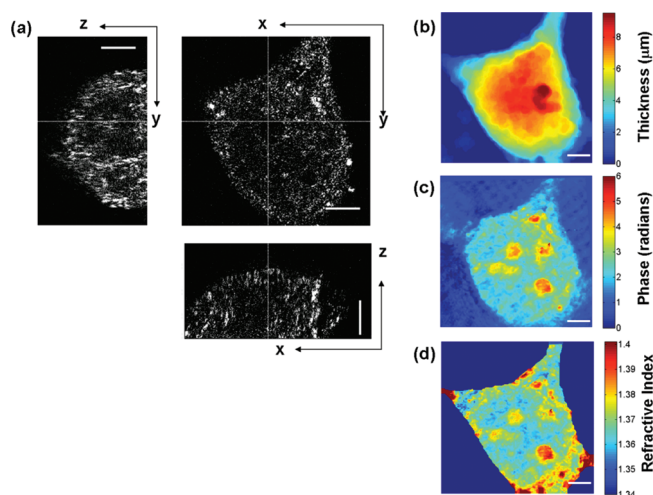


**Figure 3.** (a) Confocal reflectance images of a HeLa cell at three perpendicular planes. (b) Contour image of a HeLa cell. Color bar shows thickness in micrometers. (c) Registered 2D phase delay map of the same HeLa cell. Color bar shows phase in radians. (d) Refractive index map of the same HeLa cell. Color bar shows refractive index at wavelength of  $488\ \text{nm}$ . Scale bars in all images indicate  $5\ \mu\text{m}$ .

units of micrometers. By using one of the  $y$ – $z$  section images, we estimated the error in our contour mapping to be around  $1\ \mu\text{m}$ .

Next, we correlated the 3D confocal image with quantitative phase image (Figure 2c). Because of a mismatch in magnification and lateral position between a phase image and a confocal image, we devised a method to correct these discrepancies. A projected confocal image was generated by integrating all the lateral plane images along the  $z$  direction. This image appears similar with the quantitative phase image which is a projected image of refractive index along axial direction. Using common features from a projected confocal image and a quantitative phase image such as cell boundary and nucleolus, the correction factors including scale, position, and orientation were used to coregister both images.

From the contour map of cell boundary measured by the confocal reflectance microscopy (Figure 3b) and coregistered phase image measured by the quantitative phase microscopy (Figure 3c), we extracted the full-field map of axially averaged refractive index map,  $n_{\text{avg}}(x,y)$  (Figure 3d) through the physical relation between phase and optical path given by

$$\Delta\phi(x,y) = \frac{2\pi}{\lambda}(n_{\text{avg}}(x,y) - n_{\text{medium}})d(x,y) \quad (2)$$

where  $\Delta\phi(x,y)$  is the phase induced by the sample,  $d(x,y)$  is the cell height map,  $n_{\text{medium}}$  is the index of medium, and  $\lambda$  is the wavelength of light source. The refractive index of the culture medium has been previously measured to be  $1.34$  in the visible range.<sup>12</sup> The refractive index image shows a high contrast visualization of the cell's internal structures. The two large round circles in the image are nucleoli which are commonly found in a eukaryotic cell and possess high refractive index than the rest of the cells. The mean refractive index of the examined HeLa cell was  $1.371 \pm 0.012$ . Note that the accuracy in the axially averaged refractive index measurement was about  $0.002$ , which was estimated from the phase detection sensitivity of quantitative phase microscopy,  $10\ \text{mrad}$ , and axial resolution of confocal microscopy,  $1\ \mu\text{m}$ . The standard deviation in cell index

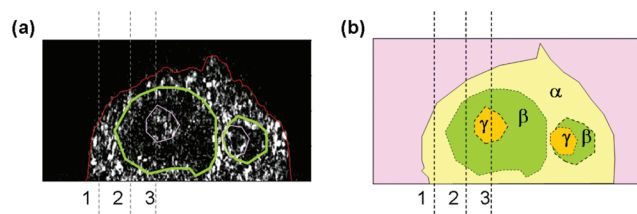


**Figure 4.** (a) Vertical section of a HeLa cell from the 3D confocal reflection image with the outlines of cell, nucleus and nucleolus superimposed. Scale bar indicates  $5 \mu\text{m}$ . (b) Diagram showing the outlines of cytoplasm ( $\alpha$ ), nucleus ( $\beta$ ), and nucleolus ( $\gamma$ ). Note that dotted lines 1, 2, and 3 in both images are selected such that line 1 consists only of cytoplasm, line 2 of cytoplasm and nucleus, and line 3 of cytoplasm, nucleus, and nucleolus.

measurements results from the heterogeneous distribution of index inside cells and is in larger than the accuracy of our system.

Confocal reflectance images provide not only the cell contour but also the internal structures of subcellular organelles of cytoplasm and nucleus. From simple calculation, we could extract also the index of the nucleus. Similarly, the index along line 3 is composed of cytoplasm, nucleus, and nucleolus. With previously calculated indices of cytoplasm and nucleus, we could determine the index of nucleolus. The measured refractive indices of cytoplasm, nuclear matrix, and nucleolus were  $1.375 \pm 0.011$ ,  $1.371 \pm 0.009$ , and  $1.38 \pm 0.008$ , respectively. Note that the standard deviations are not the accuracies of the measurements but the distribution of refractive index in the samples.

#### 4. Discussion and Conclusion

In this study, we have demonstrated that the axially averaged refractive index of a live cell can be accurately estimated by the simultaneous detection of optical and physical thicknesses using Hilbert phase microscopy and confocal reflectance microscopy, respectively. Moreover, refractive indices of intracellular organelles could be determined from the 3D image analysis of confocal reflectance maps. From the fact that the addition of 1 g of typical proteins in 100 mL of water increases the index by 0.0018–0.002,<sup>5</sup> measured cellular refractive index leads to the estimation of protein concentrations. While Hilbert phase microscopy provides the total dry mass of the cells,<sup>24</sup> our method enables the estimation of organelle-dependent protein contents. The proposed technique is not limited to biological

applications and can be extended to the chemical analysis of heterogeneous materials. Future directions will include the study of dynamics of cell metabolism (Figure 4).

**Acknowledgment.** This work was funded by the National Center for Research Resources of the National Institutes of Health (P41-RR02594-18), the National Science Foundation (DBI-0754339), and Hamamatsu Corporation. G.P. acknowledges support from NSF (CAREER: 08-46660).

#### References and Notes

- (1) Ingle, J. D.; Crouch, S. R. *Spectrochemical Analysis*; Prentice Hall: NJ, 1988.
- (2) Gore, M. G. *Spectrophotometry and spectrofluorimetry: a practical approach*, 2 ed.; Oxford University Press: Oxford, U.K., 2002.
- (3) Parnis, J. M.; Ozin, G. A. *J. Phys. Chem.* **1988**, *92*, 3959.
- (4) Rubio, N.; Sanchez-Garcia, D.; Jimenez-Banzo, A.; Rey, O.; Borrell, J. I.; Teixido, J.; Nonell, S. *J. Phys. Chem. A* **2006**, *110*, 3480.
- (5) Barer, R.; Ross, K. F. A.; Tkaczyk, S. *Nature* **1953**, *171*, 720.
- (6) Zernike, F. *Physica* **1942**, *9*, 686.
- (7) Nomarski, G. J. *Phys. Radium* **1955**, *16*, 9S.
- (8) Mazarevica, G.; Freivalds, T.; Jurka, A. *J. Biomed. Opt.* **2002**, *7*, 244.
- (9) Park, Y.; Diez-Silva, M.; Popescu, G.; Lykotraftitis, G.; Choi, W.; Feld, M. S.; Suresh, S. *Proc. Natl. Acad. Sci. U.S.A.* **2008**, *105*, 13730.
- (10) Choi, W.; Fang-Yen, C.; Badizadegan, K.; Oh, S.; Lue, N.; Dasari, R. R.; Feld, M. S. *Nature Methods* **2007**, *4*, 717.
- (11) Ikeda, T.; Popescu, G.; Dasari, R. R.; Feld, M. S. *Opt. Lett.* **2005**, *30*, 1165.
- (12) Lue, N.; Popescu, G.; Ikeda, T.; Dasari, R. R.; Badizadegan, K.; Feld, M. S. *Opt. Lett.* **2006**, *31*, 2579.
- (13) Rappaz, B.; Marquet, P.; Cuche, E.; Emery, Y.; Depeursinge, C.; Magistretti, P. *Opt. Express* **2005**, *13*, 9361.
- (14) Rappaz, B.; Charriere, F.; Depeursinge, C.; Magistretti, P. J.; Marquet, P. *Opt. Lett.* **2008**, *33*, 744.
- (15) Curl, C. L.; Bellair, C. J.; Harris, T.; Allman, B. E.; Harris, P. J.; Stewart, A. G.; Roberts, A.; Nugent, K. A.; Delbridge, L. M. D. *Cytometry Part A* **2005**, *65A*, 88.
- (16) Lichtman, J. W. *Sci. Am.* **1994**, *271*, 40.
- (17) White, J. G.; Amos, W. B.; Fordham, M. *J. Cell Biol.* **1987**, *105*, 41.
- (18) Pawley, J. B. *Handbook of Biological Confocal Microscopy*, Third ed.; Springer-Verlag: Heidelberg, Germany, 2006.
- (19) Popescu, G.; Ikeda, T.; Best, C. A.; Badizadegan, K.; Dasari, R. R.; Feld, M. S. *J. Biomed. Opt.* **2005**, *10*.
- (20) Ghiglia, D. C.; Pritt, M. D. 1998.
- (21) Piekos, W. B. *Microsc. Res. Techn.* **1999**, *46*, 334.
- (22) Sheppard, C. J. R.; Wilson, T. *Proc. R. Soc. London, Ser. a-Math. Phys. Eng. Sci.* **1982**, *379*, 145.
- (23) Brakenhoff, G. J.; Blom, P.; Barends, P. J. *Microsc.-Oxford* **1979**, *117*, 219.
- (24) Popescu, G.; Park, Y.; Lue, N.; Best-Popescu, C.; Deflores, L.; Dasari, R. R.; Feld, M. S.; Badizadegan, K. *Am. J. Physiol.-Cell Physiol.* **2008**, *295*, C538.

JP904746R